

Improved Processes to Remove Naphthenic Acids

Annual Technical Progress Report

(From October 1, 2003 to September 30, 2004)

Principle Authors

Aihua Zhang, Qisheng Ma, Kangshi Wang
William A. Goddard (PI), Yongchun Tang (co-PI),

Date Report was issued: May 5, 2005

DOE Award number: DE-FC26-02NT15383

Name and Address of Submitting Organization

California Institute of Technology
1200 East California Blvd.,
Pasadena, CA91125

Disclaimer

This report was prepared as an account of work sponsored by an agency of the United States Government. Neither the United States Government nor any agency thereof, nor any of their employees, makes any warranty, express or implied, or assumes any legal liability or responsibility for the accuracy, completeness, or usefulness of any information, apparatus, product, or process disclosed, or represents that its use would not infringe privately owned rights. Reference herein to any specific commercial products, process, or services by trade name, trademark, manufacturer, or otherwise does not necessarily constitute or imply its endorsement, recommendation, or favoring by the United States Government or any agency thereof. The views and opinions of authors expressed herein do not necessarily state or reflect those of the United States Government or any agency thereof.

Abstract

In the second year of this project, we continued our effort to develop low temperature decarboxylation catalysts and investigate the behavior of these catalysts at different reaction conditions. We conducted a large number of dynamic measurements with crude oil and model compounds to obtain the information at different reaction stages, which was scheduled as the Task2 in our work plan. We developed a novel adsorption method to remove naphthenic acid from crude oil using naturally occurring materials such as clays. Our results show promise as an industrial application. The theoretical modeling proposed several possible reaction pathways and predicted the reactivity depending on the catalysts employed. From all of these studies, we obtained more comprehensive understanding about catalytic decarboxylation and oil upgrading based on the naphthenic acid removal concept.

Table of Content

Improved Processes to Remove Naphthenic Acids

Disclaimer	2
Abstract.....	2
Table of Content.....	3
Introduction.....	4
Executive Summary	5
Experimental Methods	6
1. Total Acid Number Measurement.....	6
1.1 Procedures	6
1.2 Results	6
2. Flow Reaction Setup and Operation.....	7
3. Adsorption of Naphthenic Acids onto Clay Minerals/Adsorbent Selection and Adsorption Measurement.....	8
4. Advanced Theoretical Calculation Methods.....	9
Results and Discussion.....	10
1. More Results on the Catalytic Decarboxylation of Model Acid Compounds	10
1.1 On Rare Earth Metal Oxides	10
1.2 On Oxidative Metal Oxides	10
2. Kinetic Measurement with Crude Oil in the Presence of Solid Catalysts.....	11
3. Discovery on the Novel Naphthenic Acid Absorbents	17
4. Chemical Processes on Metal Oxide Surfaces	18
4.1 Chemical Adsorption of Carboxylic Acids on MgO(100) and CaO(100) Surfaces	18
4.2 Deprotonation Process of Carboxylic Acids on MgO(100) and CaO(100) Surfaces.....	19
4.3 Decarboxylation and Desorption Processes on MgO(100) and CaO(100) Surfaces.....	19
4.4 Energy Profits of Chemical Processes on MgO(100) and CaO(100) Surfaces.....	20
4.5 Progresses in Mechanism Studies Based on Theoretical Calculations.....	21
Conclusions.....	22
Work plan for the 3rd years (2005)	23
References.....	23

Introduction

It has been known that carboxylic acids are present in crude oil and contribute to the acidity of oil products. The existence of these compounds, e.g. naphthenic acids in oil, has been recognized as one of the major sources of corrosion that occurs in transportation pipelines and distillation units in refineries. Consequently, the oil products with high concentrations of naphthenic acid are labeled as poor oil quality and have a lower price in the market.

The conventional method to remove naphthenic acid is based on a caustic wash. However, this treatment results in the formation of emulsion. Once it is formed, this emulsion is very difficult to be broken.

The aims of the current project are to develop cost-effective methods to remove naphthenic acids from crude oil. Two objectives are targeted: (1) to develop a novel decarboxylation process through a catalytic reaction to convert these acids to non-corrosive components; (2) to remove naphthenic acids via a chemical adsorption process by using solid absorbent.

In the first year, we assembled a team combining both experimental/theoretical researchers with extended academic/industrial expertise. We established our experimental and theoretical methodologies for studies of the catalytic decarboxylation process. We developed both glass and stainless steel micro batch type reactors for the fast screening of various catalysts with reaction substrates of model carboxylic acid compounds and crude oil samples. We also developed novel product analysis methods such as GC analyses for organic acids and gaseous products. Our research revealed the effectiveness of several solid catalysts for the catalytic decarboxylation of model compounds and for the acid removal from crude oil. Our theoretical calculations propose a three-step concerted oxidative decarboxylation mechanism for one of the effective decarboxylation catalysts we developed.

In the second year of this project, we continued our effort to get more first hand results and through which, we obtained more comprehensive understanding on the catalytic decarboxylation and oil upgrading process based on this naphthenic acid removal concept.

Executive Summary

In the second year of this project, important progresses have been achieved through our continuous efforts. The major achievements of this year can be highlighted as the following:

- More oxidative metal oxide catalysts were developed that have been identified to be effective to the catalytic decarboxylation of model acid compounds. Among them, Ag₂O shows excellent decarboxylation activity for naphthoic acid at 300°C. The acid conversion, CO₂ yield and naphthalene yield reached 93.9%, 96.9% and 66.2% respectively.
- Laboratory-scale flow reaction line was established to conduct continuous evaluation of the catalytic activities. Extensive kinetic information was studied through IR adsorption of RCOO, Total Acid Number (TAN) and oil viscosity.
- The kinetic measurements were performed with MgO and MnO₂ catalysts, which represent two typical effective catalysts developed in our lab. The two catalysts can keep effective for the removal of naphthenic acids from several hrs (MnO₂) to more than 10 hrs (MgO) while the oil treatment capacities could reach about 51 and 95 g-oil/g-catalyst respectively.
- The measurement method of TAN was developed in our lab following the procedure of ASTM standard method D664. Excellent accuracy and reproducibility were verified through comparing with the data obtained from the oil service company.
- Theoretical studies of the decarboxylation mechanism suggest that i) the radical pathway will be predominant when transition metals such as Cu(II), Mn(III) are involved. These cation species are able to generate an internal electron-transfer due to the closed-shell (from Cu(II), -3d⁹ to Cu(I), -3d¹⁰ electronic configurations) and half closed-shell (from Mn(III) -3d⁴ to Mn(II) -3d⁵ electronic configurations). ii) The concerted pathways could be a rationalized mechanism when base metals are involved. In the concerted pathway, the nucleophilic attack on the β-carbon is important as the initiative step. iii) The hydroxyl group on the metal surface could assist on the decarboxylation featured the C-C bond breaking. This result seems to suggest that a basic condition is essential for the initial base-acid reaction, an acidic condition would be important for the further decarboxylation reaction.
- Several clay minerals were selected for the adsorption of naphthenic acids. Sepiolite and Montmorillonite demonstrate higher adsorptive capacities in comparison with other clays.

Experimental Methods

1. Total Acid Number Measurement

An in-house Total Acid Number (TAN) measurement method was developed following the procedure of ASTM standard method D664. The principle of this measurement is based on non-aqueous acid base potentiometric titration determined by a PH/mv meter (Oakton PH510 Series).

1.1 Procedures

The major operation steps consist of the followings.

- *Preparation of alcoholic potassium hydroxide solution* – Add 6g of KOH to approximately 1L of anhydrous iso-propanol. Boil gently for 30min to increase the solubility of KOH in the solution. Store the solution overnight and then standardize the solution with potassium acid phthalate ($\text{KHC}_8\text{H}_4\text{O}_4$ or KHP).
- *Standardization of alcoholic KOH solution* – Standardize the solution with potentiometric titration of weighed quantities of KHP dissolved in CO_2 -free water.
- *Preparation of oil sample* – Dissolve 1-5g oil sample in 125ml titration solvent (500ml toluene/495ml anhydrous iso-propanol/5ml water), filter the sample and transfer the prepared solution to a 250ml beaker, which is used as the titration vessel.
- *Titration of KOH to oil sample* – Add suitable amount of KOH alcoholic solution and wait until a constant potential has been observed, then record the solution used and meter readings. When the sample was titrated close to the inflection point, add less drops of KOH and record the meter carefully. For each set of samples, make a blank titration of the titration solvent.
- *Calculation* – Plot the volumes of KOH solution added versus the corresponding electrode potential (mv). Mark the inflection points A and B for oil sample and solvent only, which should reflect the largest potential changes for a unit KOH. Calculate the TAN as the equation

$$\text{Acid number, mg KOH/g} = (\text{A}-\text{B}) \times \text{M} \times 56.1/\text{W}$$

M: Concentration of alcoholic KOH solution, mol/L

W: Sample mass, g

1.2 Results

Two typical titration curves for KOH to KHP and KOH to oil were shown in Figure1 and Figure 2. In each case, the inflection points were clearly observed. The results we measured were consistent with the data obtained from The Oil Analysis Lab.

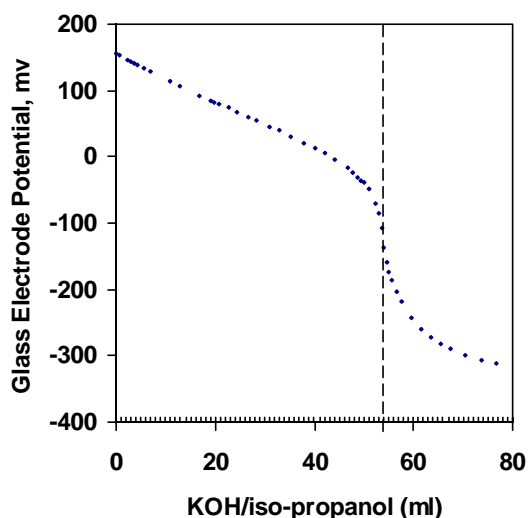


Figure 1 Titration Curve of Potassium Acid Phthalate to KOH/iso-Propanol Solution

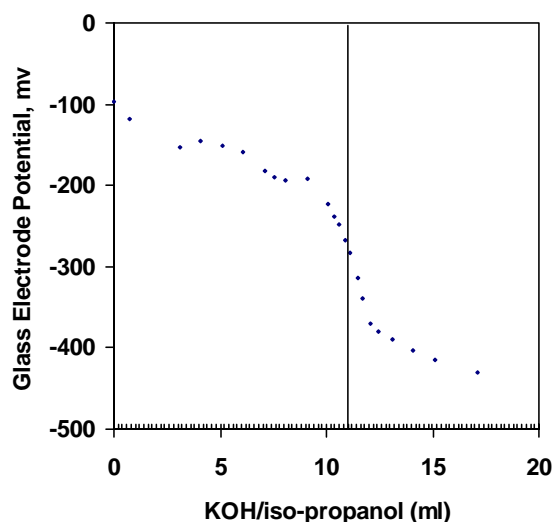


Figure 2 Titration Curve of KOH/iso-Propanol Solution to Oil Sample

	In our lab	Oil Analysis Lab
TAN	4.35 (1st), 4.29 (2nd)	4.35 (1st), 4.38 (2nd)

2. Flow Reaction Setup and Operation

To develop the catalyst with longer catalytic life and obtain the information on the reaction mechanism and reaction kinetics, which was scheduled as the Task2 in our work plan, a flow reaction system was established.

As shown in Figure 3, a liquid pump was used to pump out decane to a transfer vessel at a constant flow rate. The crude oil filled in the other side of the transfer vessel was pressed out by decane through the transfer piston. Two pressure gauges were placed in the line to monitor the flow condition. N₂ purge line was set to purge the oil out after the reaction. A stainless steel reactor with 0.4cm ID and 29cm in length was used to conduct the catalytic tests. All the transfer, tubing lines and valves were wrapped with heating tape to warm up to 80°C to keep the oil flowable.

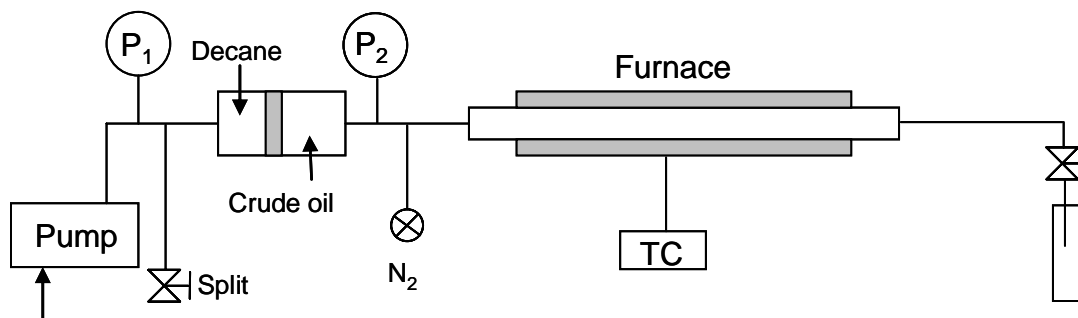


Figure 3 Flow Reaction System Setup

3. Adsorption of Naphthenic Acids onto Clay Minerals/Adsorbent Selection and Adsorption Measurement

The purpose of this study is to use clay minerals as the solid adsorbents to remove naphthenic acid. The major components of clay minerals are silica, alumina, and water, frequently with appreciable quantities of iron, alkali, and alkaline earth cations. Natural clays usually have high cation-exchange capacity (CEC) and surface areas. In addition, they are inexpensive and environmentally friendly. Clay minerals may interact with many organic compounds to form complexes of varying stabilities and properties. Clay organic interactions are multivariable reactions involving the silicate layers, the inorganic cations, water and the organic molecules. The chemical affinity between the acid compound and the solid surface depends on structure (molecular weight, chain length, etc) of the acid molecule, functional groups present in the acid molecule such as hydrophobic groups (-C-C-C-C-), electronegative groups (-C=O, -C-O-C-, -OH), π bonds (-C=C-, aromatic rings), and configuration of the acid molecule (Kowalska etc, 1994).

The model naphthenic acids (NAs) solution was prepared by using four commercial NAs (i.e. cyclohexanepropionic acid (NA1), benzoic acid (NA2), cyclohexanepentanoic acid (NA3), and 4-heptylbenzoic acid (NA4) with tetradecane dissolved in dodecane (C12). Their concentrations were about 0.5% each in weight percent. Several clay samples (from the Source Clay Repository of Clay Mineral Society at Purdue University, West Lafayette, IN), i.e. Kaolin (KGa-2), Illite (IMt-1), Illite-smectite mixed layer 60/40 (ISMt-2), Illite-smectite mixed layer 70/30 (ISCz-1), Palygorskite (PF1-1), Montmorillonite (SAz-1), Ca-Montmorillonite (SAz-2), Montmorillonite, CA (SCa-3), Sepiolite (SepSp-1), Hectorite (SHCa-1), and Na-Montmorillonite, WY (SWy-2), were chosen as model adsorbents for this study. The chemical compositions of clay minerals used are shown in Table 1. The adsorption experiments were carried out using the batch equilibration technique. Desired amounts of a NAs solution were added to different glass centrifuge tubes, which contained known amounts of clay minerals. The tubes were shaken at 25°C and 66°C for 24 hours, then followed by centrifugation for 10 min. Supernatants were sampled and subject to analysis for NAs concentrations using a Hewlett Packard Gas Chromatography-Mass Spectroscopy (GC-MS). No changes in solute concentrations without clays were detected in the tubes within the experimental period. Therefore, solute mass lost in the supernatant from clay slurries was assumed to be adsorbed by clay. The amount of NAs adsorbed was calculated from the difference between the initial and equilibrium solute concentration in dodecane solution.

Table 1 Chemical Composition of Clay Minerals

Clay code	Description	Chemical composition (%)										Cation exchange capacity (meq/100g)	Surface area (m ² /g)
		SiO ₂	Al ₂ O ₃	TiO ₂	Fe ₂ O ₃	FeO	MnO	MgO	CaO	Na ₂ O	K ₂ O		
KGa-2	Kaolinite, high defect	43.9	38.5	2.08	0.98	0.15	n.d.	0.03	n.d.	<0.005	0.065	3.3	23.5
IMt-1	Illite	49.3	24.25	0.55	7.32	0.55	0.03	2.56	0.43	0	7.83	n/a	n/a
ISCz-1	Illite-Smectite, 70/30	51.6	25.6	0.039	1.11	<0.1	0.04	2.46	0.67	0.32	5.36	n/a	n/a
ISMt-2	Illite-Smectite, 60/40	51.2	26.3	0.17	1.49	0.1	0.01	2.41	1.4	0.04	4.74	n/a	n/a
PF1-1	Palygorskite	60.9	10.4	0.49	2.98	0.4	0.058	10.2	1.98	0.058	0.8	19.5	136.35
SAz-1	Montmorillonite (AZ)	60.4	17.6	0.24	1.42	0.08	0.099	6.46	2.82	0.063	0.19	120	97.42
SAz-2	Ca-Montmorillonite (AZ)	60.4	17.6	0.24	1.42	0.08	0.099	6.46	2.82	0.063	0.19	120	97.42
SCa-3	Montmorillonite (CA)	52.8	15.7	0.181	1.06	<0.10	0.03	7.98	0.95	0.92	0.03	n/a	n/a
SepSp-1	Sepiolite	52.9	2.56	<0.001	1.22	0.3	0.13	23.6	<0.01	<0.01	0.05	n/a	n/a
SHCa-1	Hectorite	34.7	0.69	0.038	0.02	0.25	0.008	15.3	23.4	1.26	0.13	43.9	63.19
SWy-2	Na-Montmorillonite (WY)	62.9	19.6	0.09	3.35	0.32	0.006	3.05	1.68	1.53	0.53	76.4	31.82

4. Advanced Theoretical Calculation Methods

Our computational modeling is relied on a twin-prone approach. Both are based on the modern Quantum Mechanics (QM) Density Functional Theory (DFT) at the Generalized Gradient Approximation (GGA) level using the B3LYP and PBE functionals. High level QM finite clusters calculations have been carried out using the Jaguar codes, from which, the detailed decarboxylation mechanisms are investigated through calculations of structural, energetic and thermodynamic properties of all possible stable, intermediated, and transition states. In the meantime, a new computational program SeqQuest, developed by Peter Schultz at Sandia National Labs and on which we have been collaborating over years, is used to deal with 3-dimension crystal and 2-dimension slab systems. Some special features of developing SeqQuest program are shown as follows:

- *General Proposes* – can deal with 0-D (finite cluster); 1-D (polymer); 2-D (slab) and 3-D (bulk) systems
- *Multiple Functionals* – using DFT of LDA, GGA, PBE, PW91 and BLYP methods
- *Powerful* – such as automated geometry and cell optimization; ‘freeze’ selected atoms; Nudged Elastic Band (NEB) transition state finders; and molecular dynamic calculations
- *Various Build-in potentials and basis sets* – Near complete LDA atom library

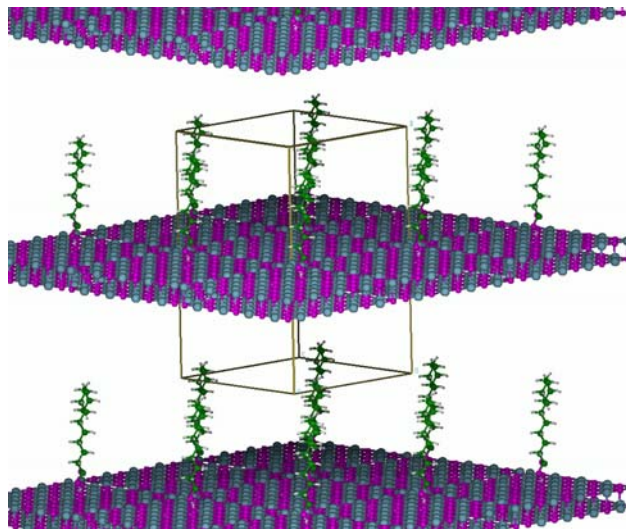


Figure 4 Adsorption of CycloHexane Carboxylate Acid (CHCA) on the MgO(100) Surface - A 2-D Slab Model

(65 atoms); and growing GGA/PBE library (20+ atoms); as well as Pseudopotentials and LCAO basis sets.

A slab model has been used to mimic chemical processes of carboxylic acids on metal oxide surface. To ensure the computational accuracy and to minimize the artificial lattice and slab interactions, a well-separated slab system is set up. For both of the MgO and CaO slabs in our calculations, we employed a double-layer $4 \times 4 \times 8 \text{ \AA}^3$ slab consisting of totally 32 atoms (\mathbf{a} is the lattice constant) for their (100) surface (Figure 1). The adsorption energy E_{ads} is defined as:

$$E_{\text{ads}} = E(\text{mole+slab}) - E(\text{slab}) - E(\text{mole})$$

Where, $E(\text{mole})$, $E(\text{slab})$ are calculated total energies (in eV, $1\text{eV}=23.07\text{ kcal/mol}$) of the separated molecule and surface slab, respectively; and $E(\text{mole+slab})$ is the total energy (in eV) of the molecule attached on the slab surface.

Results and Discussion

1. More Results on the Catalytic Decarboxylation of Model Acid Compounds

1.1 On Rare Earth Metal Oxides

Continuing the work of last year, several rare earth metal oxides, including CeO_2 , La_2O_3 , Y_2O_3 and ZrO_2 were tested with model acid, naphthoic acid ($\text{C}_{10}\text{H}_7\text{COOH}$) and the result was shown in Table 2. The low CO_2 yields, defined as the carbon conversion to CO_2 as shown in Table 2 suggest that they were inactive towards catalytic decarboxylation although the acid-base dual functionalities of ZrO_2 were expected.

Table 2: Catalytic Decarboxylation of Naphthoic Acid in the Presence of Rare Earth Metal oxides

Run #	Acid (mg)	Catalyst (mg)	Temp ($^{\circ}\text{C}$)	RT (hr)	CO_2 yield (%)		
151	NA	51.6			0.06		
152	NA	47.7	CeO_2	10.6	250	4	0.16
152	NA	49.7	La_2O_3	10.4	250	4	0.01
154	NA	50.6	Y_2O_3	10.5	250	4	0.00
155	NA	51.2	ZrO_2	11.1	250	4	0.00
177	NA	51.6	ZrO_2	13.3	300	4	0.94

NA, $\text{C}_{10}\text{H}_7\text{COOH}$, 2-naphthoic acid

1.2 On Oxidative Metal Oxides

More oxidative metal oxides were investigated in the catalytic decarboxylation of model compounds, naphthoic acid and cyclohexane pentanoic acid. The latter is considered to be more

representative as the component of naphthenic acid in crude oil. The tested metal oxides include Ag_2O , AgO , MnO_2 , Mn_2O_3 , PbO_2 , CuO , Cu_2O , Fe_2O_3 and Co_2O_3 . Note that all of these metal oxides have variable oxidative states.

The data in Table 3 show that the CO_2 formation, which is an indication of the catalytic decarboxylation, was detected in each case except for Fe_2O_3 . At the temperature of 250°C , the CO_2 yields were all lower than 10% although the acid conversion could reach higher. Increasing the reaction temperature to 300°C resulted in the higher CO_2 yields, as well as higher acid conversions, suggesting that the catalytic activities of these metal oxides are temperature sensitive. Importantly, the CO_2 yield from Ag_2O reached as high as 96.93%, indicating the naphthoic acid has been almost completely converted to CO_2 . The high acid conversion of 93.9% is consistent with these data. In addition, naphthalene, as another important decarboxylated product, was also detected. The yield of naphthalene, defined as the carbon conversion to naphthalene, reached to 66.2%. Moreover, The GC-MS analysis also identified the formation of 1, 2'-binaphthalene and 2, 2'-binaphthalene ($\text{C}_{20}\text{H}_{14}$). These byproducts might be the result of dimerization of naphthalene. This result strongly suggested that the reaction occurred through a radical mechanism.

Comparison of the same metal atoms at different oxidative states does not show a general trend on their decarboxylation efficiency. For instance, Ag(I) is much active than Ag(II) , but Mn(IV) yields more CO_2 than Mn(III) , while Cu(I) and Cu(II) gave almost equal CO_2 yields at the temperature of 300°C .

When applying Ag_2O , MnO_2 and PbO_2 to a new acid substrate, cyclohexane pentanoic acid (CHPA), CO_2 was also detected although the yields were not as high due to the lower reaction temperature. These results show promise for the application of oxidative metal oxide catalysts to react with diverse acid substrate structures.

Regarding the mechanism of catalytic decarboxylation on oxidative metal oxides, oxidative decarboxylation via radical intermediate would be the most plausible reaction path. Accordingly, the oxidative abilities of these compounds will be essential to the activities.

2. Kinetic Measurement with Crude Oil in the Presence of Solid Catalysts

To get the information based on the concept of multiple cold traps, which was scheduled in our proposal, we performed flow reaction tests as an alternative way. The TAN, oil viscosity and IR adsorption of the treated oil were measured at different reaction stages.

Two catalysts e.g. MgO and MnO_2 were investigated again. These have been recognized to be effective to the decarboxylation of model compounds and the removal of naphthenic acid from crude oil in batch reaction tests. 0.5g of the catalyst, whose particle size falls in 28-65

Table 3 Catalytic Decarboxylation of Model Carboxylic Acids in the Presence of Oxidative Metal oxides

Acid (mg)		Catalyst (mg)		Temp (°C)	RT (hr)	Acid conv (%)	CO ₂ yield (%)	C ₁₀ H ₈ Yield (%)	C ₂₀ H ₁₄
NA	60.0	Ag ₂ O	9.8	250	4	26.0	3.6		
NA	49.7	MnO ₂	10.0	250	4	34.2	3.3		
NA	56.6	Mn ₂ O ₃	10.2	250	4	20.2	2.8		
NA	50.2	PbO ₂	11.8	250	4	24.9	4.5		
NA	49.9	CuO	10.2	250	4	53.9	3.5		
NA	57.6	Cu ₂ O	10.7	250	4	59.2	6.7		
NA	49.5	Fe ₂ O ₃	9.7	250	4	40.2	0.0		
NA	55.2	Co ₂ O ₃	10.7	250	4	16.0	6.0		
NA	54.0	Ag ₂ O	10.8	300	4	93.9	96.9	66.2	detected
NA	48.3	AgO	10.2	300	4	16.1	15.4	2.2	
NA	49.7	MnO ₂	11.5	300	4	74.3	17.1	0.5	detected
NA	52.6	Mn ₂ O ₃	10.7	300	4	61.8	5.2		
NA	49.9	PbO ₂	10.8	300	4	38.4	5.2		
NA	52.2	CuO	11.5	300	4	56.5	20.9	4.4	
NA	50.2	Cu ₂ O	10.1	300	4	63.6	22.9	13.7	
CHPA	64.0	Ag ₂ O	9.4	250	4	10.6	2.8		
CHPA	65.6	MnO ₂	10.3	250	4	36.2	5.5		
CHPA	72.2	PbO ₂	13.9	250	4	24.4	5.3		

NA, C₁₀H₇COOH, 2-naphthoic acidCHPA, C₆H₁₁C₄H₈COOH, Cyclohexane pentanoic acid

mesh, was loaded in a tubular reactor and the crude oil from Texaco with 2% CHPA addition was pumped into and flew through the reactor at the flow rate about 3~4g/hr. During the reaction, IR was used to monitor the effectiveness of the catalyst. If the RCOOH adsorption significantly recovered, it is a signal that the catalyst has been deactivated and the reaction could be shut down wherein. The oils were collected at different reaction intervals and then subjected to TAN analysis and viscosity measurement after the reaction.

The thermal treatment results at different temperatures are shown in **Figure 5** and **Table 4**. IR measurement shows that the temperature effect is complicated for oil thermal treatment. It has an increase followed by decrease. The TANs for the oils treated at 250°C and 300°C were found to get higher than the starting feed. This might be due to some light components, not including naphthenic acid, were evaporated in this temperature range, and the apparent naphthenic acid concentration would get high. Further increase the temperature to 350°C, some naphthenic acids might also be evaporated or decomposed, which led to the lower acidity.

For MgO catalyst, the reaction was continuously run for 29.25hr in total (80°C for 2hr, 150°C for 2hr, 250°C for 21.33hr, and 300°C for 4hr) with the result shown in Figure 6 and Table5. The IR measurement showed that the catalyst was effective until 9hr at 250°C (totally13hr). At this time, the oil collected was 47.74g in total and the oil treatment capacity was calculated to be 95.48g-oil/g-MgO. The TAN of the oil decreased more than 30% after 13hr

in stream. It was noticed that there were some inconsistency between IR measurement and TAN analysis. Regarding this, more detailed investigation is needed.

We further increased the reaction temperature to 300°C and the oil was treated with MgO catalyst for longer time (**Figure 7 and Table 6**). IR measurement shows that the deactivation started from 12hrs 30min. The TAN measurement gave lower values of 5.6 and 7.9 for the oils collected during the reaction time 2-4 and 5-8 hrs periods, respectively. The acid conversion calculated based on TAN decrease have reached to 64-50%. If continuously increasing the reaction temperature to 350°C, the collected oil became more flowable. This led to the lower viscosity. The possible reason related to this would be the occurrence of catalytic cracking, which might be promoted by MgO.

On the role of MgO to acid removal, it is considered have multiple mechanisms. The results with model acid compound identified its decarboxylation activity, due to the CO₂ formation. Meanwhile because of its inherent strong basicity, MgO will also tend to react with acid through acid-base neutralization. At higher temperature, MgO is reported to be active to promote C-C cracking of hydrocarbons.

As our strategy has been focusing on two type catalysts, alkaline earth metal oxides and oxidative metal oxides, we chose one of them, MnO₂ to run a flow test (**Figure 8 and Table 7**). For MnO₂ catalyst, the reaction was continuously run at 250°C for 10hr30min. The IR measurement showed that MnO₂ was effective to RCOOH reduction at the early reaction stage and then the peaks increased gradually with the reaction time. After 10hr35min, it was recovered almost completely. The TAN analysis showed that TAN of the oil decreased to some degree until 4.17hr and the oil treatment capacity was around 51 g oil/g-MnO₂.

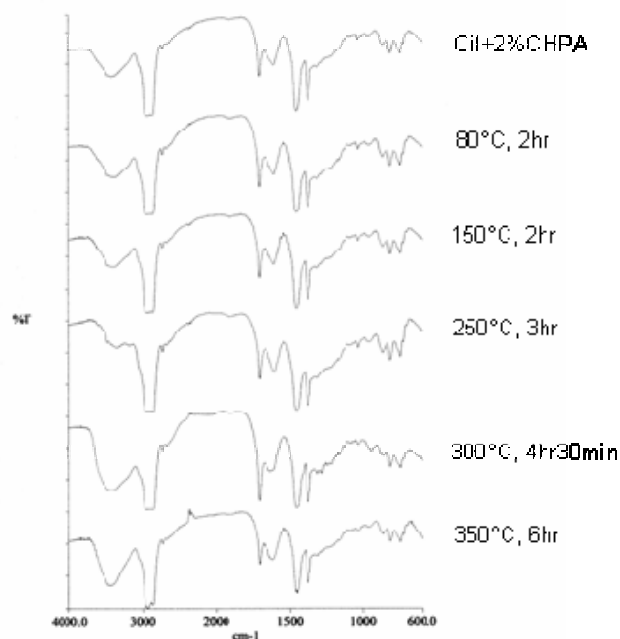


Figure 5 Thermal Treatment of Crude Oil

Table 4 TAN and Viscosity Measurement for the Thermal Treated

Temp (°C)	TAN	Viscosity (40°C / 70°C)
80	11.5	3060 / 239
150	11.1	4850 / 428
250	14.5	3720 / 368
300	15.8	3050 / 256
350	10.3	6203 / 496

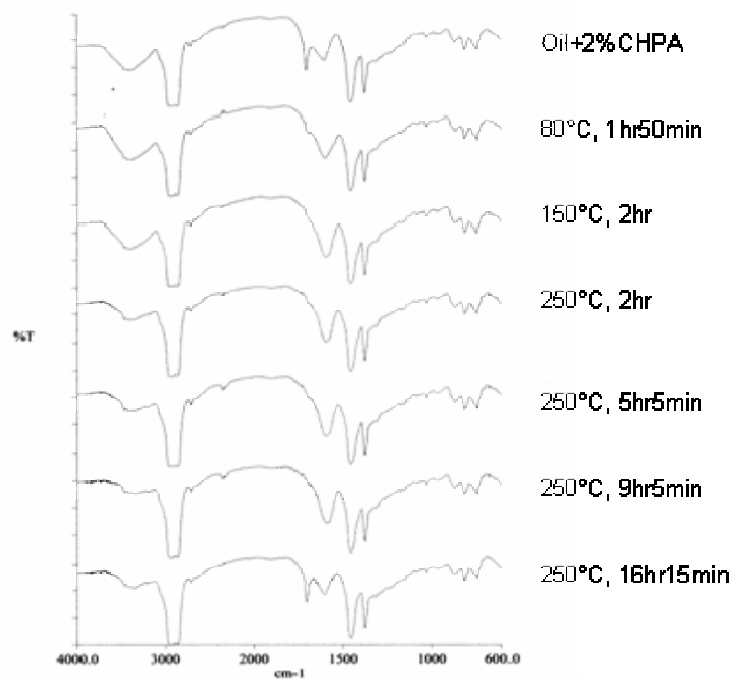


Figure 6 Flow Reaction in the Presence of MgO below 250°C

Table 5 TAN and Viscosity Measurement for the Oil Treated with MgO below 250°C

Bottle No	Oil Collecting time (hr)	Elapsed time (hr)	Temp (°C)	TAN	Viscosity (40°C)	Conv. (%)
		0		14.1	4640	
1	1.92	1.92	80	10.2		
2	2.00	3.92	150	10.3		
3	4.08	8.00	250	11.3	9120	22.1
4	5.00	13.00	250	9.3		35.9
5	5.25	18.25	250	12.8	7500	
6	5.17	23.42	250	10.1		
7	1.83	25.25	250	17.1		
8	4.00	29.25	300	10.4	3280	

MgO, 0.5mg

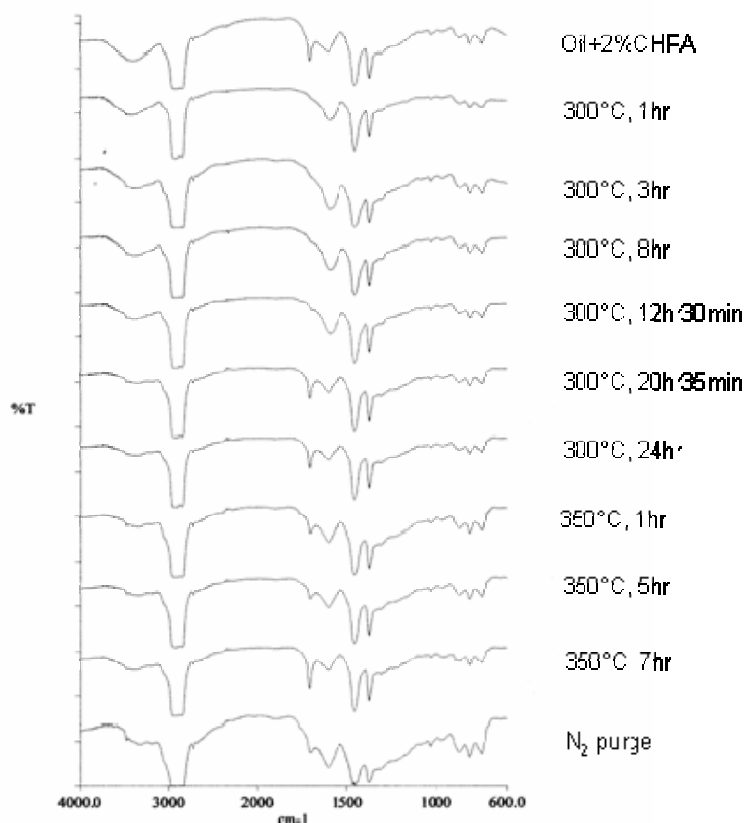


Figure 7 Flow Reaction in the Presence of MgO at 300°C and 350°C

Table 6 TAN and Viscosity Measurement for the Oil Treated with MgO at 300°C and 350°C

Bottle No.	Temp (°C)	Time Period (hr)	Oil collected (g)	Flow rate (g/hr)	IR _{RCOO}	TAN	Viscosity (40/70°C)	Conv%
Bottle 1	<300°C		5.30		weak	10.5		33.1
Bottle 2	300°C	0-1 hr	5.56	5.56	weak	8.8		44.4
Bottle 3	300°C	2-4 hr	6.17	2.06	weak	5.6		64.3
Bottle 4	300°C	5-8 hr	12.92	3.23	weak	7.9	12700 / 1040	49.8
Bottle 5	300°C	9-12.5	15.26	3.39	weak	16.9	10320 / 630	-7.5
Bottle 6	300°C	12.5-20.67 hr	27.38	3.35	strong	9.1	5020 / 376	42.2
Bottle 7	300°C	20.67-25 hr	16.34	3.70	strong	12.5	3310 / 318	20.7
Bottle 8	350°C	1-5 hr	15.70	3.14	unstable	13.7	835 / 107	
Bottle 9	350°C	6-7 hr	4.70	2.35	unstable	12.3		
Bottle 10	N ₂ purge		2.96		weak	4.1		

MgO 0.5g, 300°C, 350°C

Feed, Oil+2% CHPA

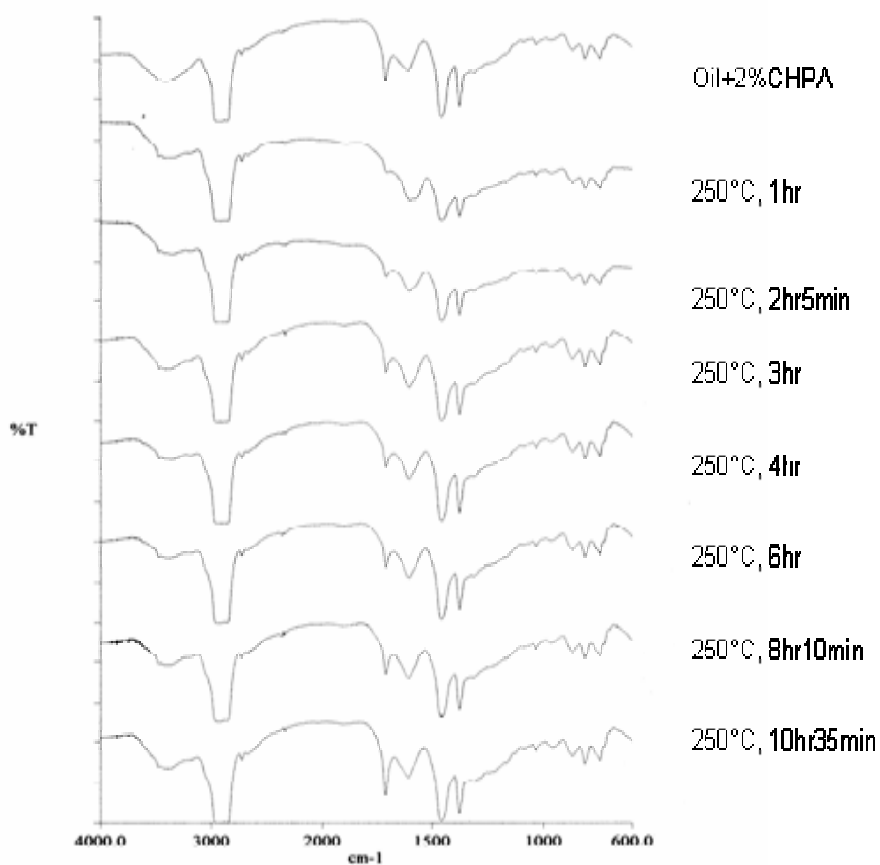


Figure 8 Flow Reaction in the Presence of MnO_2 at $250^\circ C$

Table 7 TAN and Viscosity Measurement for the Oil Treated with MnO_2 at $250^\circ C$

Flow reaction-7, MnO_2 , 0.50g

	Elapsed time (hr)	Temp ($^\circ C$)	TAN
	0	RT	14.13
	0.50	<250	11.15
0-1.17 hr	1.17	250	11.04
1.17-2.17 hr	2.17	250	12.42
2.17-4.17 hr	4.17	250	11.89
4.17-9.92 hr	9.92	250	15.27
>9.92 hr, N ₂ purge	10.30	250	9.76

Flow rate: 4.57~2.08 ml/hr

3. Discovery on the Novel Naphthenic Acid Absorbents

Table 8 summarizes the results of NAs adsorbed onto the selected clay absorbents. The order of the affinity of various clays as adsorbents to NAs is: SepSp-1>SWy-2>SAz-1>PF1-1> SHCa-1 \geq SCa-3 >SAz-2>IMt-1>IScz-1>KGa-2>ISMt-2. In addition, in each test no significant adsorption was observed for tetradecane. This result shows that these clay adsorbents are highly selective toward NAs but not hydrocarbon. This demonstrates that Sepiolite (SepSp-1) and Namontmorillonite (SWy-2) are potential efficient adsorbent for removing NAs from crude oil. The capacity of the adsorption of NAs reached 68 and 53 mg-acid/g-clay for SepSp-1 and SWy-2, respectively. On the contrary, IScz-1 was found to be inactive towards the acid adsorption. In most of clays used, the order of the affinity of four NAs adsorbed onto clays is: NA2>NA3>NA1>NA4, except onto KGa-2. The adsorption of benzoic acid onto the clays was more effective in comparison with the adsorption of other NAs. Benzoic acid with an aromatic ring showed strong effect on physical-chemical adsorption.

The current analyses of these minerals are reported as percentages of oxide, rather than as percentages of metals as shown in Table 1. We try to correlate the NA adsorption with the concentrations of MgO, CaO and Na₂O individually or with the sum of them and found the amounts of NAs adsorbed roughly increases with the amounts of MgO (Figure 9) but not related to others. We do believe that the adsorption of NAs is affected by the chemical structures of clays. We will investigate the correlation in the future study using molecular modeling.

Table 8 Efficiency of Acid Removal from the Selected Clay Absorbents

Adsorbent	NAs Adsorbed Percentage (%)				Amount of NAs Adsorbed (mg/g)
	NA1	NA2	NA3	NA4	
KGa-2	5.5	6.6	11.1	1.9	9.7
IMt-1	15.7	24.5	19.1	8.1	25.7
IScz-1	1.6	25.7	3.1	3.6	12.2
ISMt-2	0.0	0.0	0.0	0.0	0.0
PF1-1	20.1	34.3	20.2	26.9	38.9
SAz-1	21.2	46.7	23.7	13.5	40.0
SAz-2	15.4	30.8	22.3	8.5	29.3
SCa-3	16.1	30.6	19.4	8.7	34.1
SepSp-1	37.9	60.0	39.2	40.9	68.0
SHCa-1	17.4	40.4	19.4	11.8	33.9
SWy-2	17.7	47.0	23.3	49.8	53.0
NA1=Cyclohexanepropionic acid, FW = 156.23 NA2=Benzoic acid, FW = 122.1 NA3=Cyclohexanepentanoic acid, FW = 184.28 NA4=4-Heptylbenzoic acid, FW = 220.31					

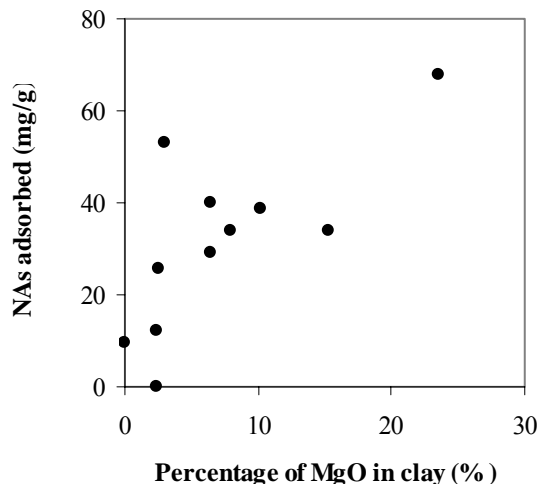


Figure 9: Correlation between NA adsorption with the percentage of MgO in clay

The crude oil (6.1g) with TAN 4.72 was added into a beaker containing 1.2g of SepSp-1 and SWy-2, respectively and then being shaken for 24 hours at 66°C. We found that the TAN was decreased to 4.03 and 3.80. However, the same amount of clay and oil, if dissolved in CH₂Cl₂, the TAN was dropped to 3.42 and 3.14, respectively at 25°C for 24 hours. Here the presence of CH₂Cl₂ is considered to have promoted the dispersion and contact between the oil and adsorbents. In another words, a good contact between the two components is necessary.

4. Chemical Processes on Metal Oxide Surfaces

4.1 Chemical Adsorption of Carboxylic Acids on MgO(100) and CaO(100) Surfaces

Both modeled aromatic (benzoic acid, BA) and saturated (cyclohexane carboxylic acid, CHCA) compounds adsorbed on the MgO(100) and CaO(100) slabs have been calculated. Table 9 shows the energies of individual compounds and the adsorption energies.

Table 9 Energies of Chemical Adsorption of Carboxylic Acids

Compounds	Calculated Energy		Adsorbed States	Calculated Energy	
	(a.u.)	(eV)		(a.u.)	(eV)
MgO-slab	-580.7883	-7898.72	BA + MgO	-731.6973	-9951.08
CaO-slab	-1230.4692	-16734.38	CHCA + MgO	-738.7742	-10047.33
BA	-150.8614	-2051.72	BA + CaO	-1381.5931	-18789.67
CHCA	-157.7015	-2144.74	CHCA + CaO	-1388.6569	-18885.73
Adsorption Energy E_{ads} (eV)					
Molecule	Slab	E_{ads}	Molecule	Slab	E_{ads}
BA	MgO	-0.65	CHCA	MgO	-3.87
BA	CaO	-3.57	CHCA	CaO	-6.61

From these results, we can see that:

- Both aromatic and saturated compounds adsorbed on MgO and CaO surfaces are energies favored;
- The adsorption of saturated compounds are even more energetic stable than aromatic compounds;
- CaO is a more effective adsorbent than MgO.

4.2 Deprotonation Process of Carboxylic Acids on MgO(100) and CaO(100) Surfaces

Deprotonation of adsorbed carboxylic acids on the metal oxide surfaces have also been calculated (Figure 10). The adsorbed state is a carboxylic ion plus a proton, with carboxylic ion attaching to the metal ion and the proton bonded to the oxygen forming a hydroxyl surface. The calculated adsorption energies as well as deprotonation energies E_{deprot} defined as:

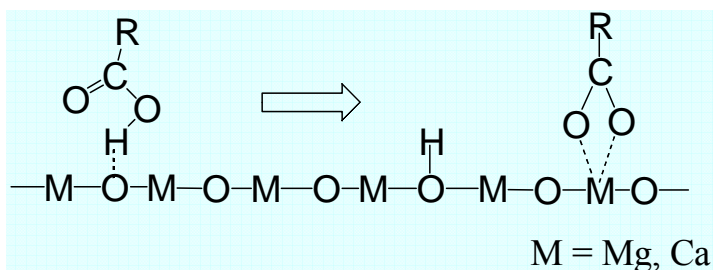


Figure 10 Deprotonation of Carboxylic Acid on Metal Oxide Surface

$$E_{\text{deprot}} = E_{\text{ads}}(\text{deprot}) - E_{\text{ads}}(\text{ads})$$

Where $E_{\text{ads}}(\text{deprot})$ and $E_{\text{ads}}(\text{ads})$ are the adsorption energies of deprotonated and un-deprotonated states, are listed in **Table 10**.

Table 10 Energies of Deprotonation of Carboxylic Acids

Compounds	Calculated Energy		Adsorption Energy	Deprotonation Energy
	(a.u.)	(eV)	E_{ads} (eV)	E_{deprot} (eV)
BA-ion + H + MgO	-731.7075	-9951.22	-0.79	-0.14
CHCA-ion + H + MgO	-738.7289	-10046.71	-3.25	0.62
BA-ion + H + CaO	-1381.5338	-18788.86	-2.76	0.81
CHCA-ion + H + CaO	-1388.5684	-18884.53	-5.41	1.20

The deprotonation energies exhibit a reversed trend as that of adsorption on both MgO(100) and CaO(100) surfaces. The less stable a carboxylic acid adsorbed on the surface, the easier it could be deprotonated. For the benzoic acid (aromatics) on the MgO surface, a negative E_{deprot} suggests that the deprotonation of BA on MgO could be an automatic process.

4.3 Decarboxylation and Desorption Processes on MgO(100) and CaO(100) Surfaces

Energetic relations of the decarboxylation and desorption processes on oxide surfaces are shown in Figure 11 and Table 11.

Table 11 Calculated Decarboxylation and Desorption Energies

Compounds	Calculated Energy		Adsorption Energy	Decarboxylation Energy
	(a.u.)	(eV)	E_{ads} (eV)	E_{decarb} (eV)
$\text{C}_6\text{H}_5^- + \text{H} + \text{CO}_2 + \text{MgO}$	-731.4026	-9947.08	3.36	4.15
$\text{C}_6\text{H}_{11}^- + \text{H} + \text{CO}_2 + \text{MgO}$	-738.3229	-10041.19	2.27	5.52
$\text{C}_6\text{H}_5^- + \text{H} + \text{CO}_2 + \text{CaO}$	-1381.2534	-18785.05	1.05	3.81
$\text{C}_6\text{H}_{11}^- + \text{H} + \text{CO}_2 + \text{CaO}$	-1388.1508	-18878.85	0.27	5.68
Compounds	Calculated Energy		Adsorption Energy	Deprotonation Energy
	(a.u.)	(eV)	E_{ads} (eV)	E_{des} (eV)
$\text{C}_6\text{H}_6 + \text{CO}_2 + \text{MgO}$	-731.6666	-9950.67	-0.23	-3.13
$\text{C}_6\text{H}_{12} + \text{CO}_2 + \text{MgO}$	-738.5552	-10044.35	-0.89	-3.16
$\text{C}_6\text{H}_6 + \text{CO}_2 + \text{CaO}$	-1381.3475	-18786.33	-0.23	-1.28
$\text{C}_6\text{H}_{12} + \text{CO}_2 + \text{CaO}$	-1388.2361	-18880.01	-0.89	-1.16

In general, the decarboxylation process requires highest energy (3~5 eV) on the oxide surfaces. This suggests that the decarboxylation process is the rate-determining step. Decarboxylation of aromatic compounds is slightly energetically favored than the saturated compounds. Desorption is an exothermal process.

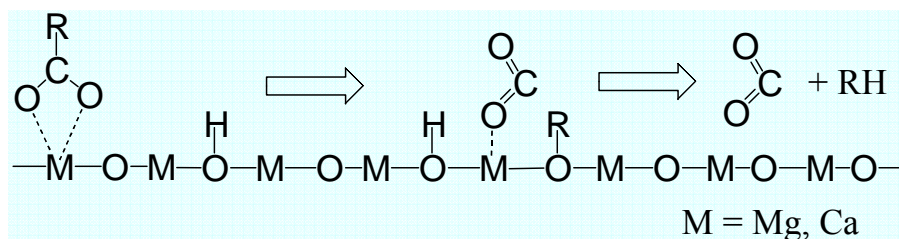


Figure 11 Decarboxylation Followed by Desorption Processes

4.4 Energy Profits of Chemical Processes on MgO(100) and CaO(100) Surfaces

The overall energy profits are summarized in Figure 12. Our results suggest that CaO will be a better solid adsorbent for the solid filtration process than MgO. However, in terms of both adsorption and decarboxylation potential, MgO is a better candidate.

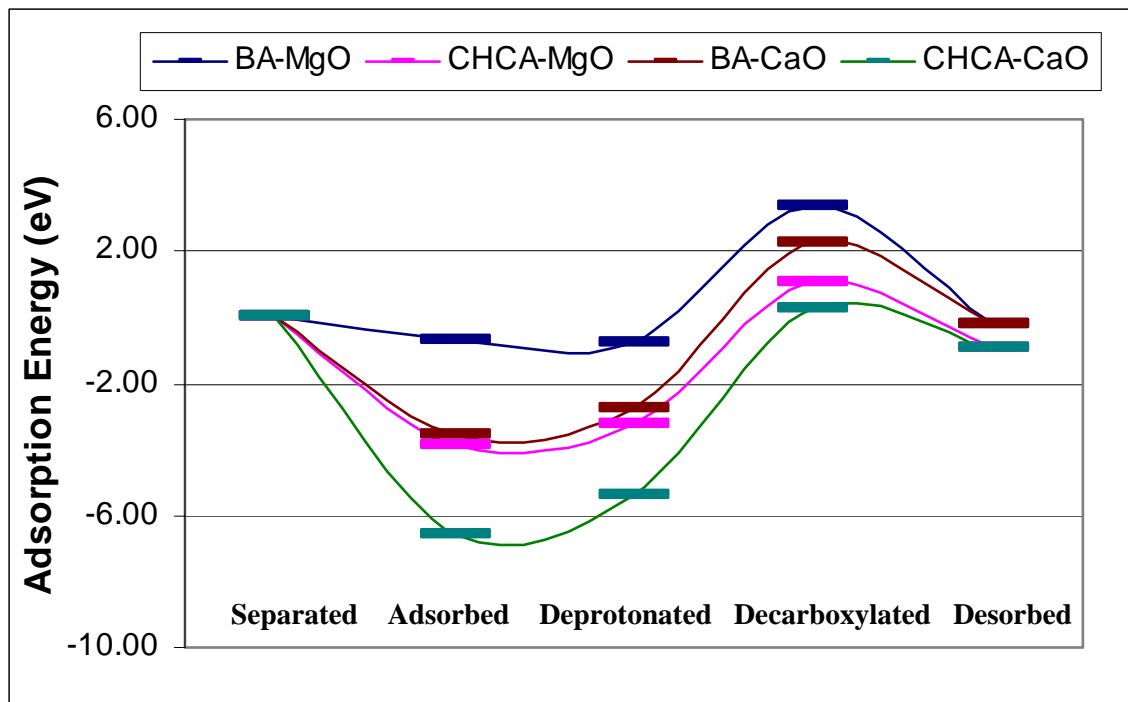


Figure 12 Calculated Adsorption Energy Eads for the adsorption, deprotonation, decarboxylation and desorption processes for both aromatics and saturates on the MgO(100) and CaO(100) surfaces

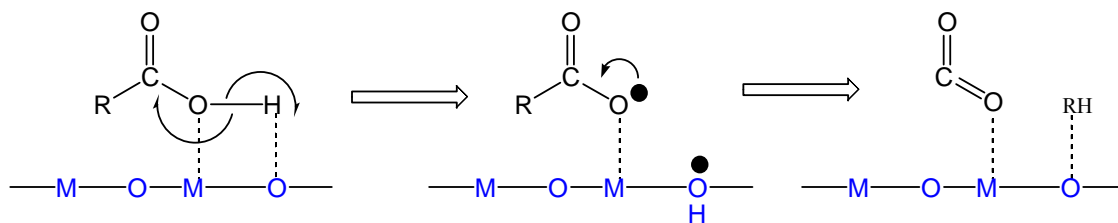
4.5 Progresses in Mechanism Studies Based on Theoretical Calculations

The theoretical study of the decarboxylation mechanism is a continuous effort of this project. Several potential decarboxylation pathways have been proposed, such as radical, cationic, anionic and concerted pathways (Figure 13). The selection of the reaction path seems to be greatly dependent on the catalytic system. This has increased the complexity of mechanistic understanding. Indeed, currently there is no a simple decarboxylation pathway that will fit into all experimental observations. However, our theoretical studies have yielded important insights into the catalyst functionality and the decarboxylation mechanism to provide more detailed understandings for the experimental chemists. For example, our theoretical studies suggested that when transition metals are involved, e.g., Cu_2O , Ag_2O , a radical pathway (pathway (1) as in Figure 13) becomes dominant. This is in consistent with our recent experimental findings that Ag_2O could cleanly decarboxylate the model compounds.

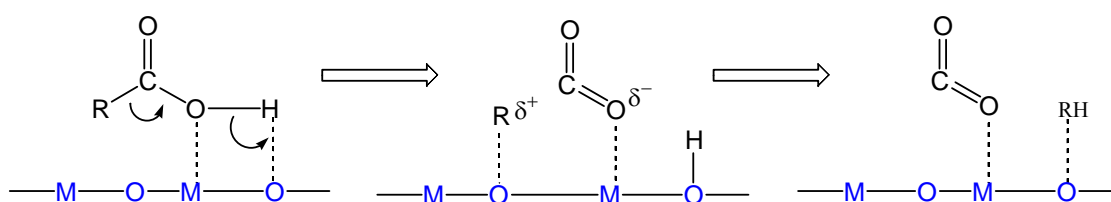
Furthermore, our calculations indicated that the deprotonation process on the MgO surface could be an automatic process (*ref.* Table 10, $E_{\text{deprot}} = -0.14$ eV). This suggested that the hydroxyl group (-OH) on the MgO surface could function as an acid site that would effectively assist the decarboxylation process (the C-C bond breaking). Therefore, the decarboxylation process on the MgO surface would likely undergo a concerted reaction pathway (pathway (3) as in Figure 13). This result is in a very good agreement with our experimental findings that MgO exhibited good characters in both of adsorption and decarboxylation toward naphthenic acid

compounds. It also suggested that an acidic solid (such as acid-types of Zeolite) could be the good candidate for the decarboxylation process.

(1) The Radical Pathway



(2) The Cationic Pathway



(3) The Anionic Pathway and/or Concerted Pathway

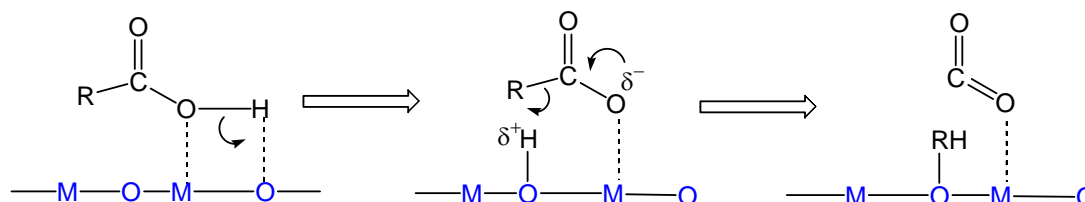


Figure 13 Proposed Decarboxylation Pathways

Conclusions

Through our continuous effort working on this project in the past two years, we have obtained a series of valuable results and comprehensive understanding on catalytic decarboxylation, NA removal via catalytic and adsorption ways. Kinetic and mechanism study as well as theoretical modeling also received important progress.

Two type catalytic decarboxylation catalysts were developed, which have features of either basic such as MgO or oxidative such as Ag₂O. It was found that MgO can promote catalytic decarboxylation, acid-base neutralization and C-C cracking to some degree, Ag₂O shows excellent decarboxylation activity for naphthoic acid model compound, from which the acid conversion, CO₂ yield and naphthalene yield reach 93.9%, 96.9% and 66.2% respectively.

Both of these two type catalysts exhibited positive effects when applied to crude oil tests. They can keep effect to reduce TAN from several hrs (MnO_2) to more than 10 hrs (MgO) while the oil treatment capacities could reach to about 51 and 95 g-oil/g-catalyst respectively.

Theoretical studies suggest that the radical pathway will be predominant when transition metals such as Cu (II), Mn (III) are involved, while the concerted pathways would be a rationalized mechanism when basic metal oxides are involved.

Several recent studies have shown the capacity of clay minerals in the adsorption of naphthenic acids. We found that Sepiolite and Na-Montmorillonite have higher adsorption capacities (AC) than other selected clays. The maximum ACs was 68mg/g for Sepiolite, and 53mg/g for Na-Montmorillonite.

Work plan for the 3rd years (2005)

Our efforts for the 3rd years of this project will follow the outline as proposed in our proposal to i) continue our modeling efforts to interpret the mechanism of naphthenic acid adsorption on solid phase; ii) conduct more naphthenic acid adsorption measurement on solid surfaced; and iii) develop and optimize a process for efficiently removing naphthenic acids from crude oil, based on the experimental and computational results.

References

- 1) N. A. Tomczyk, R. E. Winans, J. H. Shinn and R. C. Robinson, *Energy & Fuels*, 2001, 15, 1498-1504.
- 2) Mark P. Barrow, Liam A. McDonnell, Xidong Feng, Jeremie Walker and Peter J. Derrick, *Anal. Chem.* 2003, 75, 860-866.
- 3) Derungs, W. A. *Corrosion*, 1956, 12, 617t-622t.
- 4) Gutzeit, *J. Mater. Perform.* 1977, 16, 24-35.
- 5) Piehl, R. L. NACE Conference, Corrosion/87, 1987, paper No. 196.
- 6) D 664-95 in 1999 Annual Book of ASTM Standards, Section 5, Petroleum Products, Lubricants, and Fossil Fuels, Volume 05.01, 262-267.
- 7) US Patent, 4,119,440.

- 8) F. P. W. Agterberg, W. L. Driessen, J. Reedijk, H. Oevering and W. Buijs, in *New Developments in Selective Oxidation II*, Edited by Corberan and S. Vic Bellor., 1994 Elsevier Science B.V. 639-645.
- 9) Leon M. Stock and Marcus Obeng, *Energy & Fuels*, 1997, 11, 987-997.
- 10) Grim, R. E., in *Clay Mineralogy*. Edited by McGraw Hill, New York, N.Y., 1968.
- 11) Kowalska, M., Güler, Hülya, Cocke, D. L., *The Sci. of the Total Environ.*, 1994, 141, 223-240.
- 12) M.N. Ringnalda, et al., Jaguar v3.0, Portland, Oregon: Schrodinger, Inc (1997).
- 13) P.A. Schultz, M.P. Sears, & P.J. Feibelman, Quest, Albuquerque, NM: Sandia National Labs, 1998.
- 14) W. G. Toland, *J. Am. Chem. Soc.*, 83 (1961) 2507.
- 15) Agterberg et al, *New Developments in Selective Oxidation II*, *Stud. Surface Sci. Cat.* 1994, 82, 639-646.